Journal of Advanced Research in Fluid Mechanics and Thermal Sciences

Journal homepage:
https://semarakilmu.com.my/journals/index.php/fluid_mechanics_thermal_sciences/index
ISSN: 2289-7879

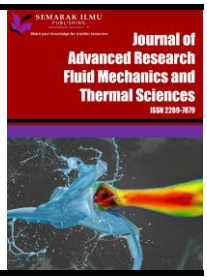

Investigation of the Influence of Bulbous Bow on the Wake Field and Power Demand

Alaaeldeen Mohamed Elhadad[1,*], Ahmed Mokhtar Abo El-Ela[1], Mohamed Mostafa Hussien[1]

[1] Shipbuilding Engineering Department, Military Technical College (MTC), Cairo, Egypt

ARTICLE INFO

Article history:
Received 22 June 2024
Received in revised form 17 October 2024
Accepted 25 October 2024
Available online 10 November 2024

Keywords:
Combatant ship; total resistance; wake field; Bulbous bow; CFD

ABSTRACT

Ship resistance is one of the main factors affecting the ship's design and the selection of her propulsion system. Propeller designers must accurately estimate the wake field in waves behind the ship in order to create effective propeller geometry under actual operating circumstances. In this study, various bulbous bow shapes of the DTMB 5415-51 surface combatant were numerically investigated using a CFD method. The aim of the study is the evaluation of the impact of the bulbous bow shape variation not only on the ship resistance but also on the wake field as well as on the propulsion performance. Three-dimensional URANS numerical flow simulations of combatant ship were applied and systematically altered bow shapes in calm water and waves were carried out. For the validation of the numerical simulations, three alternative mesh sizes for Froude numbers ranging from 0.10 to 0.40 are considered; results are compared with those of the towing tank in terms of wave field, resistance coefficients, and propulsive efficiency. The results show a considerably different hydrodynamic characteristics for different bow shapes.

1. Introduction

Although the effective wake is more relevant for the hydrodynamic efficiency of the propeller, the nominal wake flow is often used, as this can be determined independently of the propulsion system used. Therefore, the nominal wake is mostly focused on previous studies of propeller performance and wake-adapted propeller design [1]. The wake also has diverse characteristics, depending on the various types of ship geometry as taken from Yang and Kim [2]. Several numerical studies on the predictions of the hydrodynamic performance of the combatant surface ship DTMB 5415 as a benchmark ship, were presented at the Tokyo and Goteborg conferences in 2005 and 2010 respectively, and research on the wake dispersion of the propeller disc has been a focus from van Walree *et al.,* [3] and Diez *et al.,* [4]. Considerable progress has been made in numerical approaches to predict the wake field at a model scale [5]. The same applies to the simulation of ship flow fields and the prediction of total resistance, as demonstrated by earlier studies [6].

* *Corresponding author.*
E-mail address: dr.aladdinahmed@gmail.com

https://doi.org/10.37934/arfmts.123.2.140152

In this study, numerical simulation analysis for the wake flow field of DTMB 5415-51 has been performed using the CFD method. The original DTMB hull form and the DTMB with the bow modified are two distinct hull shapes that are investigated in this work [7]. These two hull shapes are compared regarding the drag at a certain speed range and the wake field. To assess the results' correctness, the RANSE solver StarCCM+ and the CAD Maxsurf software are applied.

To investigate the viability of the numerical technique, the calculation results of the hull model resistance are compared with experimental results at various speeds. The ITTC guidelines for model tests are followed and the investigations are conducted to model speed (V_m) of 0.25–2.0 m/s, equal to Froude numbers (Fr) of 0.05–0.40, in the resistance calculations. The nominal wake field was calculated using a single-phase flow model and the influence of the grid structure and the turbulence model on the calculation results were examined. To analyze and replicate how the model's wake contours formed, a sensible calculation strategy was utilized.

The goal of this study is to investigate the effect of a spherical bow on the wake field and power consumption [8,9]. It is imperative to make extensive efforts to evaluate and verify computational data. Results from the large experimental program are shown, serving as a baseline for the verification of numerical approaches. The transient nominal wake field distribution and nominal wake fraction were analyzed.

2. Mathematical Model and Governing Equations

The commercially available CFD code StarCCM+ is applied to analyze the flow of the configurations developed based on the DTMB 5415-51 model. In the numerical simulation, the continuity equation and the Reynolds-averaged Navier-Stokes equation (RANS) are solved to maintain the mass and momentum conservation. They are expressed as

$$\frac{\partial \mathrm{u_i}}{\partial \mathrm{x_i}} = 0 \tag{1}$$

$$\frac{\partial \mathrm{u_i}}{\partial \mathrm{t}} + \mathrm{u_i}\frac{\partial \mathrm{u_i}}{\partial \mathrm{x_j}} + \frac{\partial \overline{\mathrm{u_i' u_j'}}}{\partial \mathrm{x_j}} = -\frac{1}{\rho}\left(\frac{\partial \mathrm{P}}{\partial \mathrm{x_j}}\right) + \frac{\partial \tau_{\mathrm{ij}}}{\partial \mathrm{x_j}} \tag{2}$$

where *i*, *j* = 1, 2, 3 and x_1, x_2, x_3 denote horizontal, vertical, and transverse dimensions, respectively, u_i denotes the i^{th} velocity, $\overline{u_i' u_j'}$ defines the Reynolds stress component with u_i' is the fluctuating part of the velocity, p denotes the pressure, ρ stands for the density. τ_{ij} is the mean viscous stress tensor components. To solve the governing Eq. (1) and Eq. (2), the simulations employ the semi-implicit method for the pressure-linked equations (SIMPLE) algorithm [10]. The SST k − ω turbulence model of the transport equation is expressed as

$$\frac{\partial}{\partial \mathrm{t}}(\rho k) + \frac{\partial}{\partial \mathrm{xi}}(\rho k \mathrm{ui}) = \frac{\partial}{\partial \mathrm{xj}}\left(\Gamma k \frac{\partial \mathrm{k}}{\partial \mathrm{xj}}\right) + \Gamma \mathrm{k} - \mathrm{Yk} \tag{3}$$

$$\frac{\partial}{\partial \mathrm{t}}(\rho \omega) + \frac{\partial}{\partial \mathrm{xi}}(\rho \omega \mathrm{ui}) = \frac{\partial}{\partial \mathrm{xj}}\left(\Gamma \omega \frac{\partial \omega}{\partial \mathrm{xj}}\right) + \Gamma \omega - \mathrm{Y}\omega + \mathrm{S}\omega \tag{4}$$

where k denotes the turbulent kinetic energy and ω denotes the dissipation rate. Γ_k, Γ_ω, G_k, G_ω, Y_k, Y_ω and S_ω denote the production, dissipation, and cross-diffusion terms of k and ω, respectively. The Volume of Fluid (VOF) is utilized to accurately capture the free surface behavior of the two-phase

flow consisting of water and air [11]. Especially, the transport equation of two phases of water and air is given as

$$\frac{\partial \alpha}{\partial t} + \frac{\partial (\alpha u_i)}{\partial x_j} = 0 \tag{5}$$

where the volume fraction α stands for the fluid's volumetric ratio. In particular, the conditions $0 \leq \alpha \leq 1$ where $\alpha = 1$ or 0 denote that the cell is occupied by the air or water phases, respectively. The High-Resolution Interface Capturing (HRIC) system is used to model the convective flow of immiscible fluid components, and this method is appropriate for keeping track of sharp interfaces [12]. A second-order implicit technique is employed for the temporal discretization. All case studies retain a Courant Friedricks Lewey (CFL) value that is less than 0.5. Five inner iterations are employed for each time step to guarantee the nonlinear equations' convergence.

3. Grid Generation, Solution Domain, and Boundary Conditions

Surface Combatant DTMB Model 5415-51, a well-known test model, is mathematically given with an analytical description. This combatant hull is frequently used as a test case to validate numerical methods for flow simulations. Two ship models are the original DTMB and the DTMB with the bow modified. The two ship models' grid structures, attributes which correspond to a scale of 51.254, are shown in Figure 1 and Figure 2 and listed in Table 1 [13].

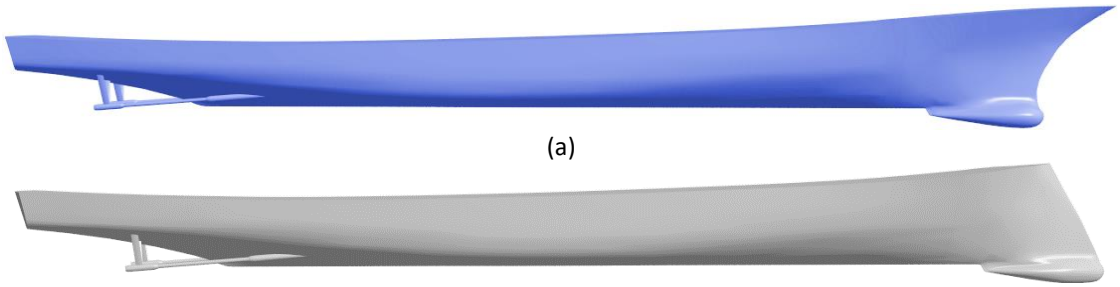

(a)

(b)

Fig. 1. (a) Original DTMB 5415-51 and (b) modified model's geometry

Table 1
The main particulars of the ship models

Parameters	Original DTMB5415-51	DTMB with the bow modified
L_{pp} (m)	2.78	2.78
B (m)	0.403	0.403
D (m)	0.244	0.244
T (m)	0.120	0.120
Δ (kg)	63.5	63.5
LCG (m)	1.375	1.375
Wetted Surface Area (S) (m^2)	1.313	1.316
Block Coefficient (C_B)	0.506	0.506

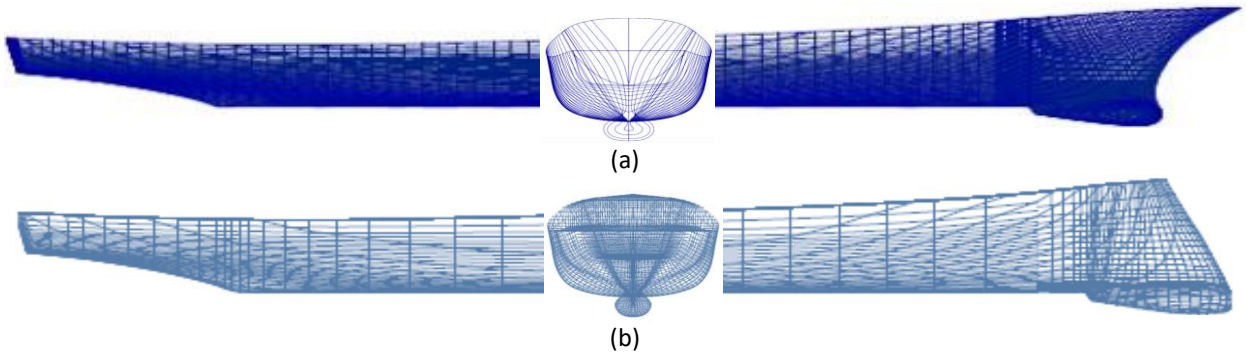

Fig. 2. (a) Lines plan and numerical grid of DTMB 5415-51 hull surface (b) Lines plan and numerical grid of modified model

The computation domain with a rectangular shape, is divided into a water and an air zone. In the Cartesian coordinate system, the x-axis is positioned to point towards the bow, the y-axis to portside, and the z-axis is positioned to point upward. According to Figure 3, The computational domain around the ship model is approximately Lm < X < −4 Lm, 0 < Y < Lm, and −Lm < Z < 0.5 Lm for length, width, and depth, respectively [14]. The inlet and outlet boundary conditions upstream and downstream are regarded as velocity inlet and pressure outlet respectively, while the flow velocity is assumed to be equal to the model speed used in the experimental investigation's speed [15]. On all outer surfaces, symmetry, and the ship hull, no-slip conditions are applied. Fr range from 0.05 to 0.40. The computations are conducted for the various hull forms investigated in the present study.

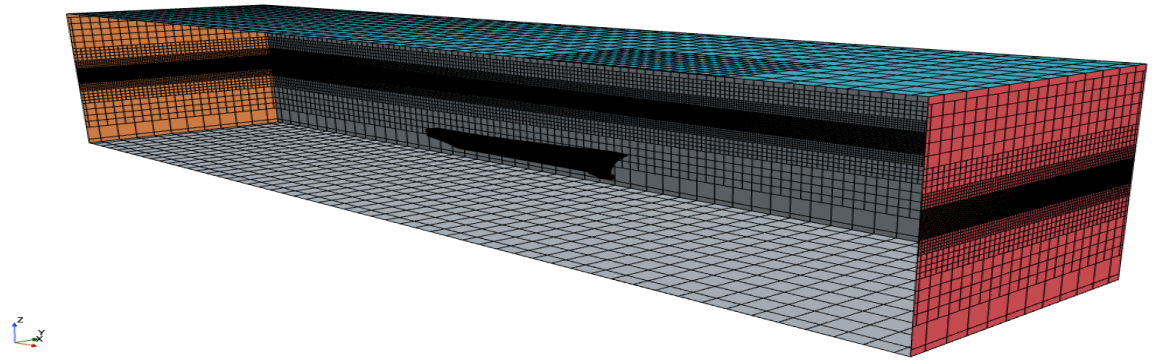

Fig. 3. Hull domain volume for the modified model geometry

The domain volume is split up into several subvolumes to provide a structured multi-block grid. The grid resolution is increased in the boundary and the free-surface elevation regions. The computational domain was discretized using hexahedral components. The minimum grid spacing of the hull wall is 1×10^{-3} L_{PP}. Figure 4 depicts the locations of the ship model relative to the various solution domain boundaries as well as a general perspective of the mesh surrounding the ship model. In the present research, a time step of 0.005 s is used, and at each time step, a maximum of 10 inner iterations are carried out [16]. A value of y+ between 30 and 100 is adopted. In this investigation, three different mesh sizes are applied with a total element count of 0.65 M, 1.95 M, and 3.8 M for coarse, medium, and fine grids respectively. Due to the ship symmetry only, a half ship is considered in the ship geometry.

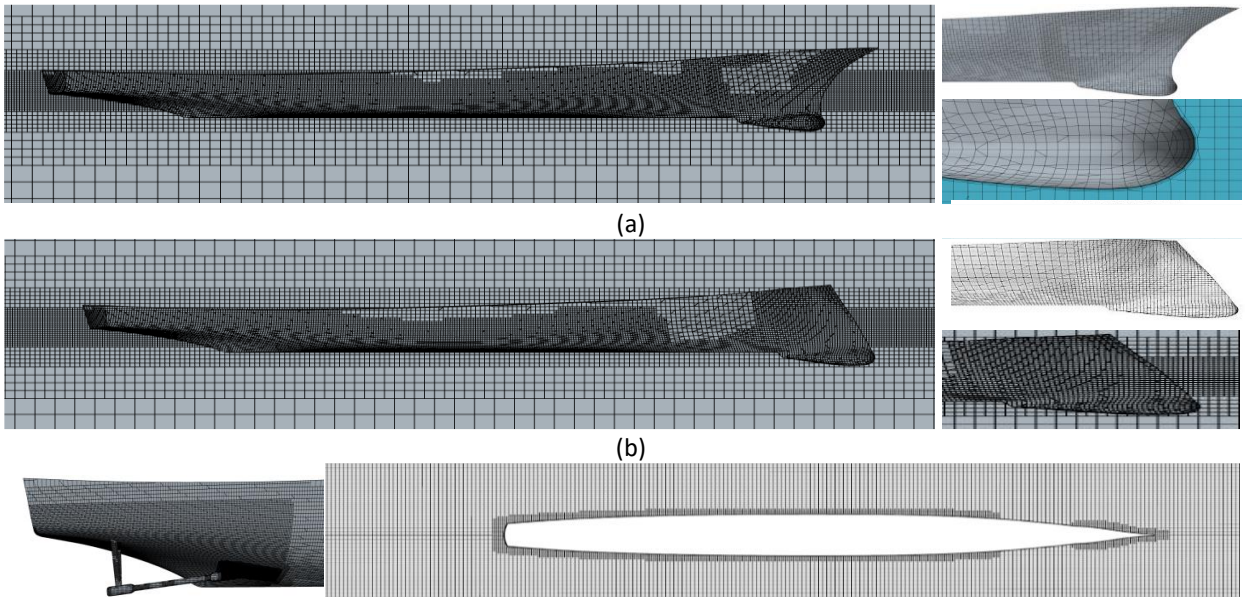

Fig. 4. Hull domain volume for (a) Original DTMB 5415-51 and (b) modified model's geometry

Between the different grids, a refinement factor of c = 1.25 uniformly specified for all spatial directions is considered. To evaluate the discretization errors, one method was used. This method produced good, consistent predictions for a variety of transient problems, including those investigated in a research by ITTC [17]. The method demanded that the same refinement factors be applied to all dimensions and that spatial and temporal refinements be performed concurrently [18]. To well capture the high-velocity gradients near the rectangular, 2 refinement blocks have been applied around and near the wake regions. To improve the computational efficiency, the coarse grid could be used in the region far away from the interesting region of the ship [19].

The uncertainty analysis of the meshes is conducted via three solutions on different mesh resolutions. The refinement ratios of these three meshes are defined as

$$r_{k+1,k} = \left(\frac{N_K}{N_{K+1}}\right)^{\frac{1}{3}} \quad (6)$$

with k = 1, 2, where N1, N2, and N3 denote the total numbers of mesh for fine, medium, and coarse meshes respectively. It is recommended $r_{k+1,k} > 1.1$ by Samion *et al.,* [20] in point of the computational cost and time consumption. The Grid Convergence Index (GCI) is defined via

$$GCI_{k.k+1} = \frac{F_s}{r^p - 1}\left|\frac{f_{k+1} - f_k}{f_k}\right| \times 100 \quad (7)$$

where $F_s = 1.25$, f_k denotes the numerical results corresponding to different meshes, p denotes the observed order of convergence and is defined as

$$p = \frac{\ln[(f_3 - f_2)/(f_2 - f_1)]}{\ln r} \quad (8)$$

The convergence condition is evaluated with the convergence ratio R

$$R = \frac{f_1 - f_2}{f_2 - f_3} \quad (9)$$

where $R < 0$, $0 < R < 1$, or $R > 1$ respectively corresponds to the oscillatory, monotonic convergence or divergence. The uncertainty of the CFD flow computation is analyzed in Table 2 for the total resistance R_t of the ship model at Fr = 0.35. Table 2 shows the Grid Convergence Index GCI of the fine mesh where GCI < 2% for the total drag R_t. This illustrates that the fine mesh is appropriate for the CFD flow computations of R_t according to the ITTC guidelines and the updated version. Moreover, the convergence ratio $0 < R < 1$ indicates that the monotonic convergence is satisfied for the CFD flow computation of the R_t at Fr = 0.35. Therefore, the fine mesh is used hereafter for the CFD flow computations of this research.

Table 2
The uncertainty analysis of the total drag Rt is based on the mesh dependency for the ship model at Fr = 0.35

Mesh	N_k	$F_k = R_t$ (N)	$r_{k+1,k}$	GCI (%)	R
Fine	3.8	9.652	1.249	1.802	0.313
Medium	1.95	9.958	1.442	5.588	--
Coarse	0.65	10.937	--	--	--

4. Resistance Calculations

The total resistance of the original DTMB 5415-51 is calculated and the results are compared with those obtained in the experimental investigation conducted in the towing tank experimental results of the MTC-TT as shown in Figure 5 [21]. In the investigations, Fr ranging from 0.10 to 0.40 are considered. The discrepancy between calculations and experiment results is determined to be less than 4%. The numerical calculation results of ship resistance with automatic running attitude adjustment are displayed in Table 3 where the difference is calculated from the following equation [22]

$$\Delta R_T\% = (R_T^{StarCCM+} - R_T^{exp})/ R_T^{exp}. \quad ??? \tag{10}$$

Table 3
The comparison of experimental and CFD results for the original model

Fn	0.10	0.15	0.20	0.25	0.30	0.35	0.40
$\Delta R_T\%$	5.477	2.35	1.48	4.03	2.69	3.15	1.87

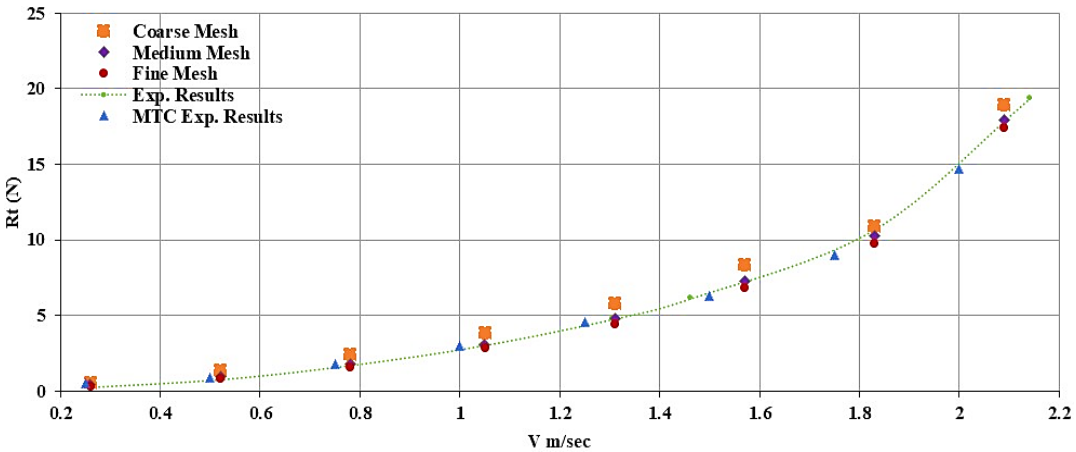

Fig. 5. Comparison of experimental and CFD results for DTMB 5415-51

The close agreement between the numerical predictions and the experimental results leads to the conclusion that the resistance prediction is possible with the entire numerical scheme and the setup used. The results for the fine and medium grids are quite similar, and the difference between the medium and coarse grids is comparatively larger but still tolerably acceptable. As a result, the fine grid fits the computations best and produces the most relevant results compared to the experimental results. Since convergent results are produced as the cell size decreases, the fine grid is used for the other DTMB hull form with the bow modified using Star CCM+.

A second phase involved utilizing CFD to determine the modified model's resistance with Fr ranging from 0.10 to 0.40 under identical conditions for fine mesh, as illustrated in Figure 6 where the values were compared to Holtrop method results used by Maxsurf. The calculated resistance values of both hull models are compared as illustrated in Figure 7. The difference in total resistance between the two hulls is small. The expected resistance differs only slightly and by the same order of magnitude. As a result, the numerical approach applied can be used to predict the resistance of the modified form.

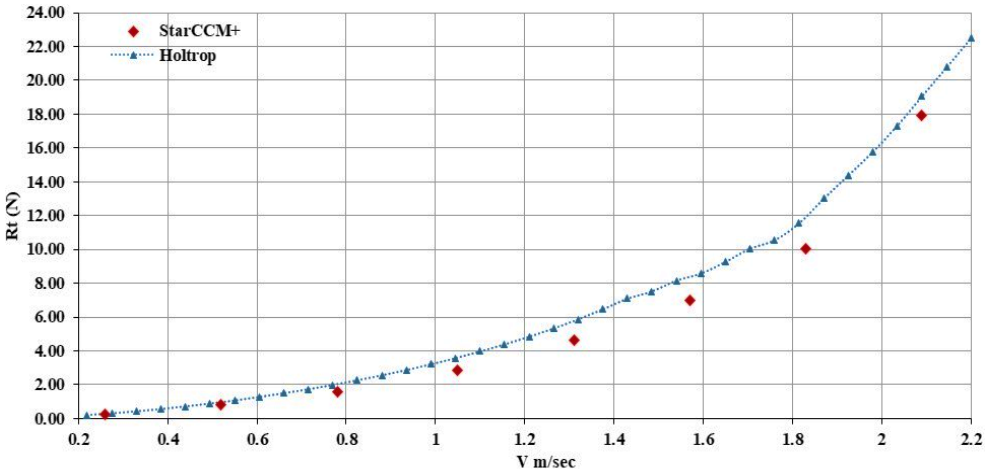

Fig. 6. Resistance over the speed for the modified hull form

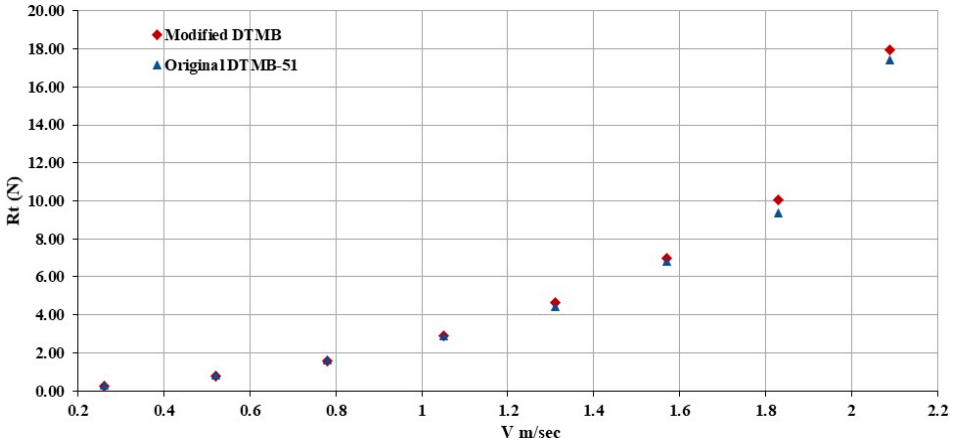

Fig. 7. The curves of total resistance for both hull models

The total viscous and residual resistance coefficients (C_{TM} C_v and C_R vs. Fr, respectively, are shown in Figure 8. Also, viscous resistance has been calculated according to the ITTC 57 formula. When Fr is in the range between 0.1 and 0.15, C_{TM} gradually drops, remains constant between 0.15 and 0.25, gradually increases between 0.25 and 0.35, and rapidly increases when Fr is greater than 0.35. For Fr

values of 0.1 to 0.35, and Fr greater than 0.35, C_R is essentially piecewise linear with a rising slope. The presence of humps and hollows is minimal in both situations.

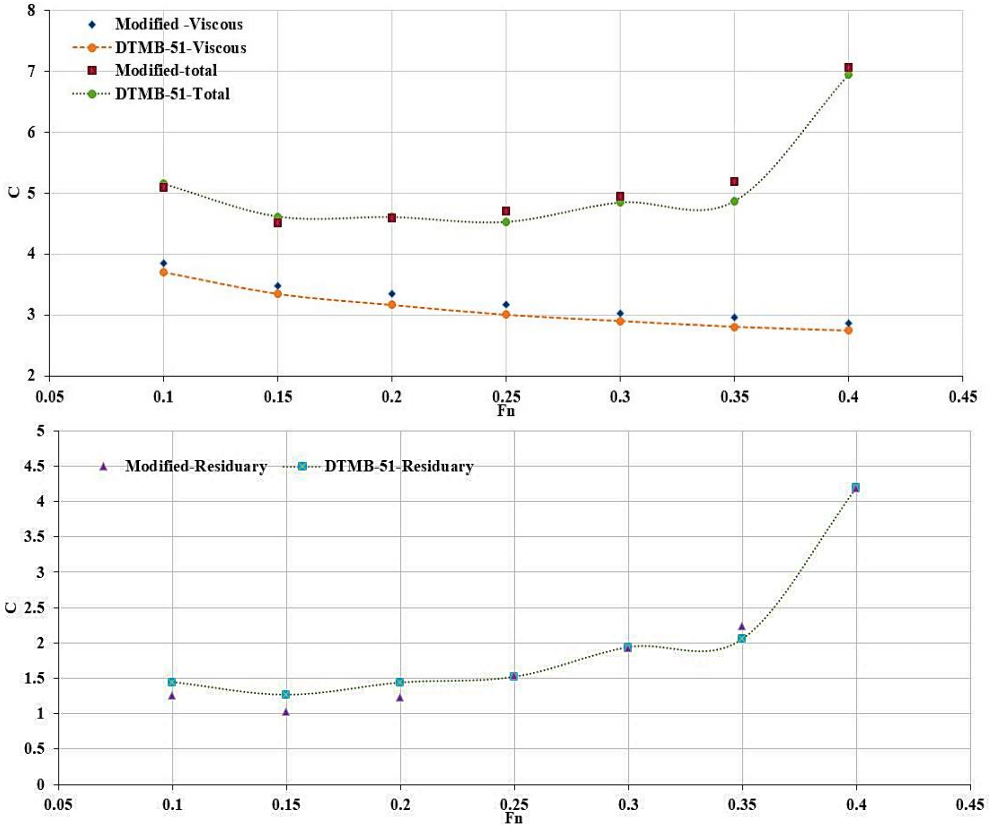

Fig. 8. The total and residuary resistance coefficients C_{TM} and C_{FM}

The numerical calculation results of hull resistance with physical time are displayed in Figure 9 whereas the mesh dependency of the modified hull model at Fr 0.25 and 0.35 is shown in Figure 10.

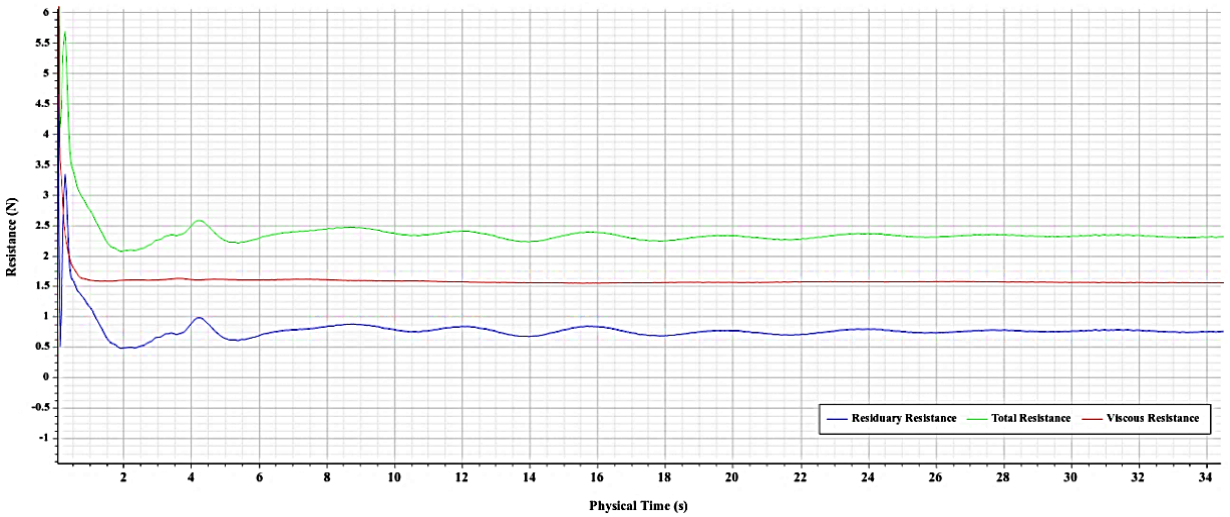

Fig. 9. Resistance plot for modified hull model at Fr = 0.25 at fine grid

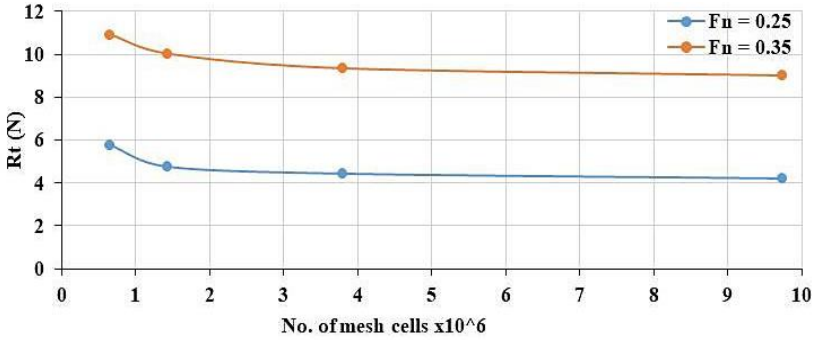

Fig. 10. Mesh dependency of the modified hull model

Finally, Figure 11 and Figure 12 illustrate the contours for the free surface wave for the two hull models at Fr = 0.25.

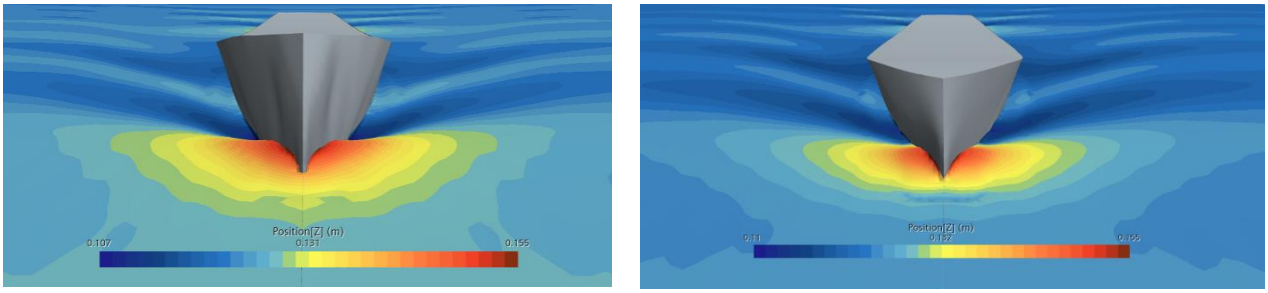

Fig. 11. Free surface wave for original Hull at RHS and Modified Hull at LHS at Fr = 0.25 [Front view]

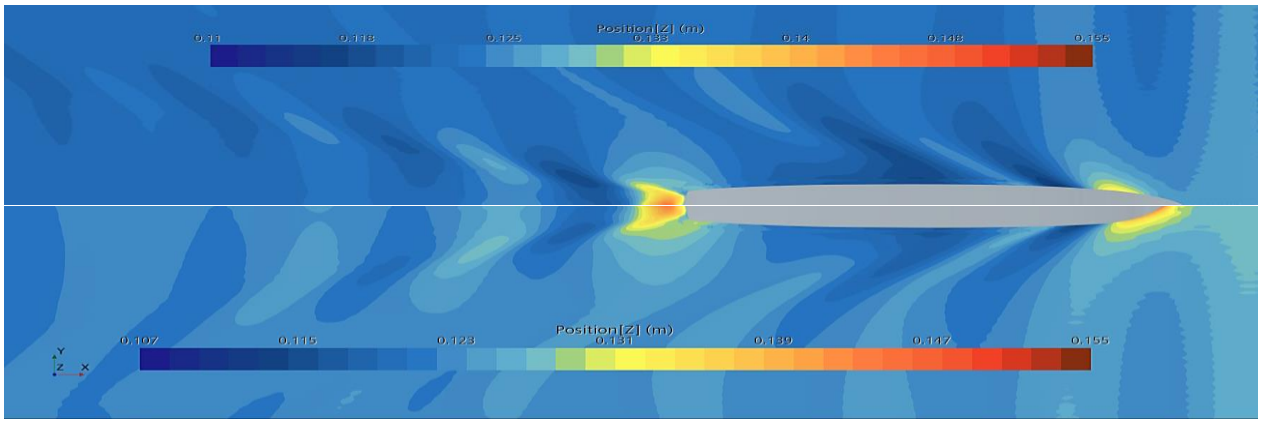

Fig. 12. Free surface wave for original Hull at the upper half and for Modified Hull at the lower half at Fr = 0.25 [Top view]

5. Wake Field Comparison

The wake distribution in the propeller plane is non-uniform due to the effect of the hull shape and the propeller shaft. The axial and the tangential wake have a strong influence on the propeller performance as they influence the efficiency, cavitation, noise, and vibration [23].

The nominal wake fraction (ω_T) on the propeller disc at radius r is given by the following equations

$$\omega_T' = \frac{1}{2\pi}\int_0^{2\pi} \omega_T'' d\theta \tag{11}$$

$$\omega_T = \frac{\int_{r_B}^{R} \omega_T' \cdot r \cdot dr}{1/2(R^2 - r_B^2)} \quad (12)$$

And, the local wake fraction can be calculated as:

$$\omega_T'' = \frac{u_s - u_a}{u_s} \quad (13)$$

where ω_T is the mean wake fraction at each radius, the local wake fraction, u_a is e axial velocity, and u_s is ship speed, giving the wake distribution.

In the present study, the nominal wake field data in the propeller disc is exported on a polar 20 × 24 grid with an angle step of 15 degrees. The 480 points in which the data is exported are shown in Figure 13. After exporting the local wake fraction for each point, the mean wake fraction is calculated. The comparison between the original and modified bulbous bow models is conducted at two speeds Fr = 0.25 and 0.35. It was observed that, the mean nominal wake fraction is quite similar for both hull forms at Fr = 0.25 with a slight increase for the modified bow shape, see Figure 14. However, for higher velocity (Fr = 0.35), the modified bow shape has considerably higher wake fraction values than the original one.

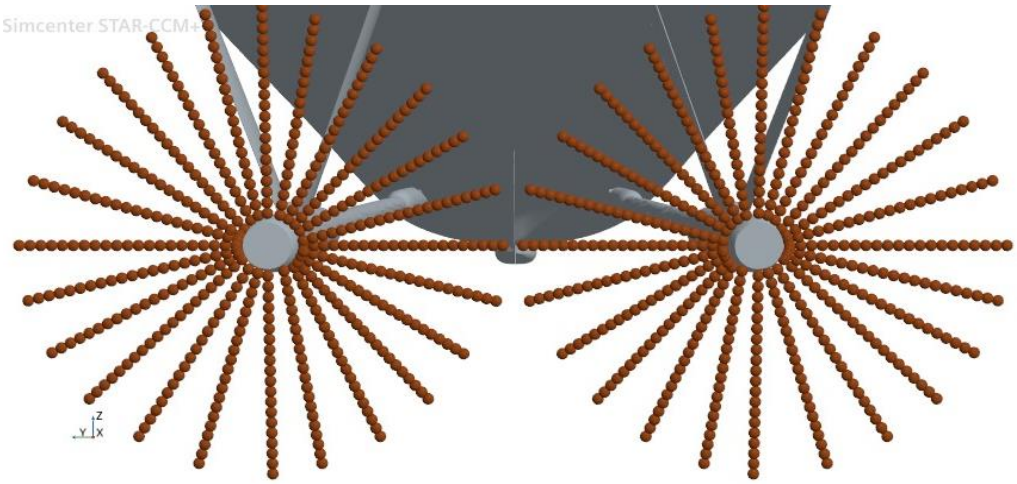

Fig. 13. The data extraction points grid located (brown dots) in each propeller disc seen from aft

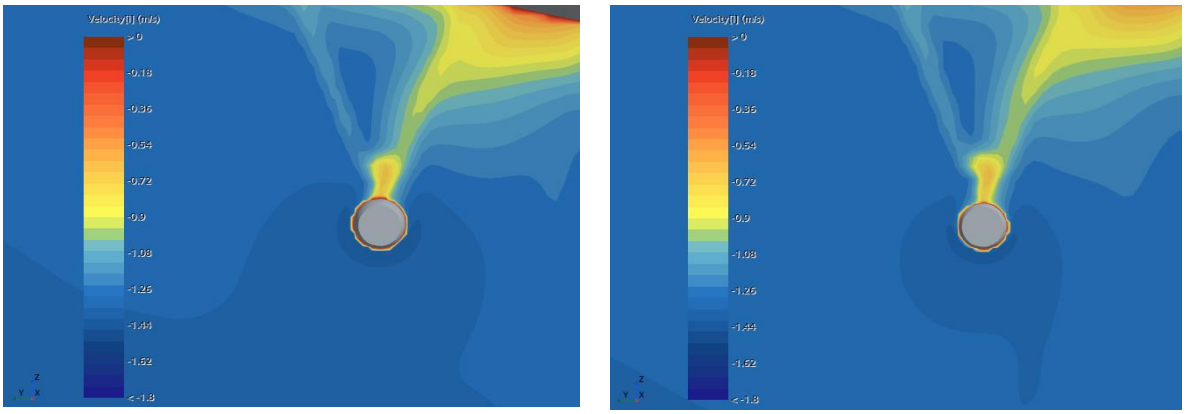

Fig. 14. Axial Velocity component for original bow shape at LHS and modified bow shape at RHS at Fr=0.25

Figure 14 and Figure 15 show the axial velocity and the axial wake fraction distributions for both hull forms. A comparison of the calculated axial wake fraction is given in Table 4. It can be seen that the wake resulting from the modified hull shape is more pronounced than that of the original shape.

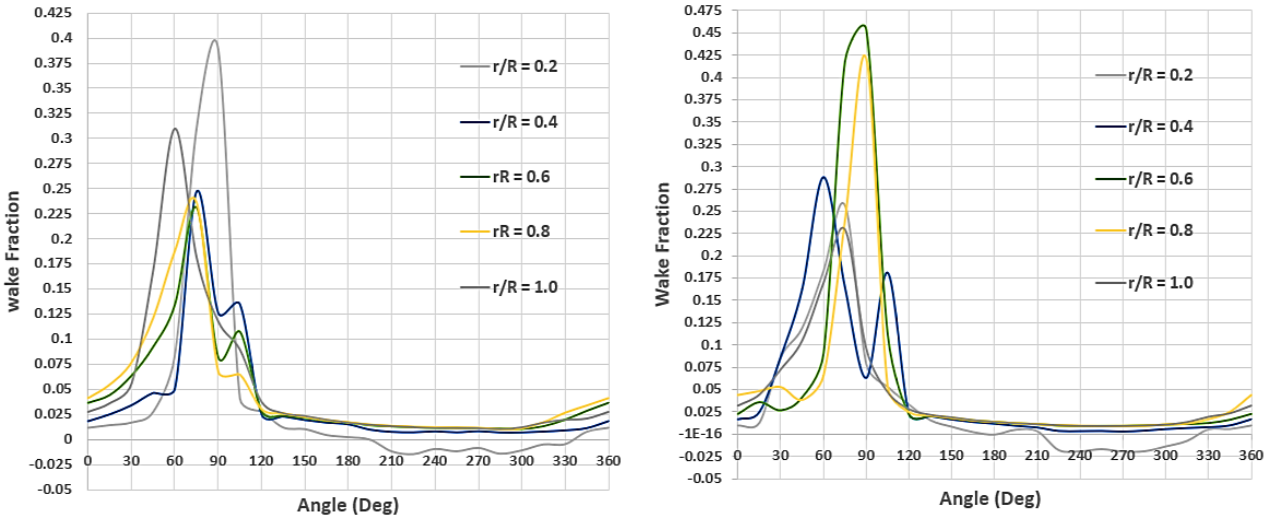

Fig. 15. Axial wake fraction distribution for original bow shape (LHS) and modified bow shape (RHS) at Fr=0.25

Table 4
The comparison between wake fraction coeff. of original and modified bow shape models

	Original	Modified	Original	Modified
Fn	0.25		0.35	
ω_T	0.45655	0.46557	0.45106	0.45968
Diff %	1.9752		1.9111	

6. Conclusion

Two DTMB ship models have the same stern form but different bow shapes were investigated. In the comparison, two aspects are considered; ship resistance and wake fraction. The numerical simulations conducted are based on RANS equations in combination with the VOF two-phase flow model. A verification study is carried out to estimate the spatial and temporal discretization error, which is less than 2.5%. The results of the numerical investigation showed a good agreement with the experimental results presented in the literature.

The results show that the new bulbous bow shape affected both the pressure distribution and the wave pattern at the free surface. Hence, an appropriate bulbous bow shape could be developed to considerably reduce the total resistance. Furthermore, the modified bulbous bow shape has a significant influence on the nominal wake fraction. The axial wake fraction at the propeller disk is slightly higher for the modified ship than the original one. The radial and tangential wake fractions did not show any significant changes and were quite similar for both ship models.

According to the current research, the new bulbous bow form has a higher wake fraction than the original, which means that it has a thicker boundary layer and slightly higher resistance. Finally, further investigations on regular and /or irregular waves are in the future study proceeding.

References

[1] Regener, Pelle Bo, Yasaman Mirsadraee, and Poul Andersen. "Nominal vs. effective wake fields and their influence on propeller cavitation performance." *Journal of Marine Science and Engineering* 6, no. 2 (2018): 34. https://doi.org/10.3390/jmse6020034

[2] Yang, Kyung-Kyu, and Yonghwan Kim. "Numerical analysis of added resistance on blunt ships with different bow shapes in short waves." *Journal of Marine Science and Technology* 22 (2017): 245-258. https://doi.org/10.1007/s00773-016-0407-9

[3] van Walree, Frans, Andrea Serani, Matteo Diez, and Frederick Stern. "Prediction of heavy weather seakeeping of a destroyer hull form by means of time domain panel and CFD codes." In *Proceedings of the 33nd Symposium on Naval Hydrodynamics*, Osaka, Japan. 2020.

[4] Diez, M., A. Serani, E. F. Campana, F. Stern, and E. F. Campana. "CFD-based stochastic optimization of a destroyer hull form for realistic ocean operations." In *14th International Conference on Fast Sea Transportation*, Nantes, France. 2017.

[5] Deshpande, Sujay, P. Sundsbø, and Subhashis Das. "Ship resistance analysis using CFD simulations in Flow-3D." *The International Journal of Multiphysics* 14, no. 3 (2020): 227-236. https://doi.org/10.21152/1750-9548.14.3.227

[6] Kuroda, Mariko, Masaru Tsujimoto, Noriyuki Sasaki, Shigeo Ohmatsu, and Ken Takagi. "Study on the bow shapes above the waterline in view of the powering and greenhouse gas emissions in actual seas." *Proceedings of the Institution of Mechanical Engineers, Part M: Journal of Engineering for the Maritime Environment* 226, no. 1 (2012): 23-35. https://doi.org/10.1177/1475090211424116

[7] Diez, Matteo, Andrea Serani, Emilio F. Campana, Omer Goren, Kadir Sarioz, D. Bulent Danisman, Gregory Grigoropoulos et al. "Multi-objective hydrodynamic optimization of the DTMB 5415 for resistance and seakeeping." In *SNAME International Conference on Fast Sea Transportation*, p. D021S005R012. SNAME, 2015. https://doi.org/10.5957/FAST-2015-034

[8] Putra, Eka Suendra, Eko Charnius Ilman, and Ahmad Fitriadhy. "Computational Investigation into Bilge Keel Effect on a Traditional Phinisi Boat's Resistance." *Journal of Ship and Marine Structures* 1, no. 1 (2023): 23-32.

[9] Nasirudin, Ahmad, I Ketut Aria Pria Utama, Sutiyo Sutiyo, and Andreas Kukuh Priyasambada. "CFD Analysis into the Resistance Estimation of Hard-Chine Monohull using Conventional against Inverted Bows." *CFD Letters* 15, no. 6 (2023): 54-64. https://doi.org/10.37934/cfdl.15.6.5464

[10] Lee, Cheol-Min, Jin-Won Yu, Jung-Eun Choi, and Inwon Lee. "Effect of bow hull forms on the resistance performance in calm water and waves for 66k DWT bulk carrier." *International Journal of Naval Architecture and Ocean Engineering* 11, no. 2 (2019): 723-735. https://doi.org/10.1016/j.ijnaoe.2019.02.007

[11] Ferziger, Joel H., Milovan Perić, Robert L. Street, Joel H. Ferziger, Milovan Perić, and Robert L. Street. "Solution of the Navier-Stokes Equations: Part 1." *Computational Methods for Fluid Dynamics* (2020): 183-226. https://doi.org/10.1007/978-3-319-99693-6_7

[12] Mikkelsen, Henrik, Yanlin Shao, and Jens Honoré Walther. "Numerical study of nominal wake fields of a container ship in oblique regular waves." *Applied Ocean Research* 119 (2022): 102968. https://doi.org/10.1016/j.apor.2021.102968

[13] Zhang, XinLong, Ping Li, and Simone Mancini. "Numerical investigation into the resistance performance for the damaged DTMB 5415 ship in calm water and regular head waves." *Ships and Offshore Structures* 17, no. 11 (2022): 2442-2453. https://doi.org/10.1080/17445302.2021.2000264

[14] Elhadad, Alaaeldeen Mohamed, Ahmed Mokhtar Abo El-Ela, and Mohamed Mostafa Hussien. "Matlab Implementation using Holtrop and Mennen Method of Bare Hull Resistance Prediction for Surface Combatant Ship Coupled with CFD." *CFD Letters* 15, no. 10 (2023): 1-11. https://doi.org/10.37934/cfdl.15.10.111

[15] Samuel, Samuel, Muhamad Fadil Audianzah, Eko Sasmito Hadi, Muhammad Luqman Hakim, Muhammad Iqbal, and Zhang Yongxing. "Verification of Ship Resistance under Calm Water Conditions through Numerical Method." *Journal of Ship and Marine Structures* 1, no. 1 (2023): 33-45.

[16] Ahmed, Alaaeldeen Mohamed Elhadad. "Comparative investigation of resistance prediction for surface combatant ship model using CFD modeling." *Journal of Advanced Research in Fluid Mechanics and Thermal Sciences* 107, no. 2 (2023): 225-235. https://doi.org/10.37934/arfmts.107.2.225235

[17] International Towing Tank Conference (ITTC). "Uncertainty Analysis in CFD Verification and Validation Methodology and Procedures." *ITTC - Recommended Procedures and Guidelines 7.5-03-01-01*, 2008.

[18] Visonneau, Michel, Ganbo Deng, Emmanuel Guilmineau, Alban Leroyer, Patrick Queutey, and Jeroen Wackers. "Computational fluid dynamics for naval hydrodynamics." *Comptes Rendus. Mécanique* 350, no. S1 (2023): 1-19. https://doi.org/10.5802/crmeca.162

[19] Serani, Andrea, Frederick Stern, Emilio F. Campana, and Matteo Diez. "Hull-form stochastic optimization via computational-cost reduction methods." *Engineering with Computers* 38, no. Suppl 3 (2022): 2245-2269.

https://doi.org/10.1007/s00366-021-01375-x

[20] Samion, Siti Ruhliah Lizarose, Nur Haziqah Shaharuddin, and Mohamed Sukri Mat Ali. "Grid convergence study for detached-eddy simulation of flow over rod-airfoil configuration using OpenFOAM." In *IOP Conference Series: Materials Science and Engineering*, vol. 491, no. 1, p. 012023. IOP Publishing, 2019. https://doi.org/10.1088/1757-899X/491/1/012023

[21] Ahmed, Alaaeldeen Mohamed Elhadad, and Ahmed Mokhtar Abo El-Ela. " Experimental and CFD Resistance Validation of Naval Combatant DTMB 5415-51 Model." *Journal of Advanced Research in Fluid Mechanics and Thermal Sciences* 107, no. 2 (2023): 84-102. https://doi.org/10.37934/arfmts.107.2.84102

[22] Żelazny, Katarzyna. "A method of calculation of ship resistance on calm water useful at preliminary stages of ship design." *Zeszyty Naukowe Akademii Morskiej w Szczecinie* 38 (110 (2014): 125-130.

[23] Neitzel, Jan Clemens, Markus Pergande, Stephan Berger, and Moustafa Abdel-Maksoud. "Influence of the numerical propulsion modelling on the velocity distribution behind the propulsion device and maneuvering forces." In *Fourth International Symposium on Marine Propulsors*, vol. 15. 2015.